Journal of Biomolecular NMR, **13:** 263–274, 1999.
KLUWER/ESCOM

Alternative E.COSY techniques for the measurement of $^3J(C'_{i-1},C^\beta_i)$ and $^3J(H^N_i,C^\beta_i)$ coupling constants in proteins

Frank Löhr & Heinz Rüterjans*
Institut für Biophysikalische Chemie, Johann Wolfgang Goethe-Universität Frankfurt am Main, Biozentrum N230, 1. OG, Marie Curie-Straße 9, D-60439 Frankfurt, Germany

Received 31 August 1998; Accepted 3 December 1998

Key words: Desulfovibrio vulgaris flavodoxin, E.COSY, ϕ-torsion angle, three-bond coupling constants

Abstract

Experiments are proposed for the measurement of the vicinal coupling constants between β-carbons and either amide protons of the same or carbonyl carbons of the preceding amino acid residue in $^{13}C/^{15}N$-labeled proteins. Both couplings depend on the backbone torsional angle ϕ. The three-dimensional pulse sequences give rise to E.COSY-like multiplet patterns in which heteronuclear one-bond couplings separate the doublet components corresponding to the two spin states of the respective passive nuclei. Thus, in contrast to previously published pulse schemes which employed the homonuclear $^1J(C^\alpha,C^\beta)$ interaction, difficulties due to overlap of spectral regions of active and passive spins are avoided. A major drawback of the novel sequences is their limited sensitivity. Nevertheless, application to *Desulfovibrio vulgaris* flavodoxin yielded coupling constants for more than 85% of all non-glycine and non-proline residues.

Introduction

The reliability of torsion angle determinations from *J* coupling information improves as the number of accessible coupling types sensitive to rotations about the same bond increases (Bystrov, 1976; Cowburn et al., 1983; Schmieder and Kessler, 1992). Owing to different phase relations the inherent degeneracy of Karplus equations which relate vicinal coupling constants with the intervening dihedral angle (Karplus, 1959, 1963) can be resolved. Also, as has been recently demonstrated for the protein backbone angle ϕ (Hu and Bax, 1997; Schmidt et al., 1999), Karplus parametrizations can be achieved without taking recourse to X-ray structural information when experimental data for all six associated vicinal couplings is available. Two of these couplings include the $^{13}C^\beta$ nucleus, and E.COSY-type (Griesinger et al., 1985, 1986, 1987) methods have been devised for their measurement (Löhr and Rüterjans, 1995; Wang and Bax, 1996; Löhr et al., 1997), exploiting the $^1J(C^\alpha,C^\beta)$ interaction to separate the multiplet components corresponding to the α and β spin states of the β-carbon. A problem common to these experiments is that pulses on $^{13}C^\alpha$, required for the coherence transfer to the vicinal coupling partner of the β-carbons (i.e. $^{13}C'_{i-1}$ or $^1H^N_i$) inevitably lead to a perturbation of the passive spin states in amino acid residues such as serine and threonine whose $^{13}C^\alpha$ and $^{13}C^\beta$ resonance regions overlap. This difficulty does not occur for quantitative *J* correlation schemes suitable for the measurement of $^3J(C'_{i-1},C^\beta_i)$ (Hu and Bax, 1997; Konrat et al., 1997), but very small coupling constants may not be detectable because of sensitivity limitations. Finally, $^3J(H^N_i,C^\beta_i)$ coupling constants can be extracted from intraresidual H^N-H^β cross peaks in 2D NOESY (Wagner, 1990) or 3D ^{15}N-separated NOESY-HMQC spectra (Seip et al., 1994) exhibiting an E.COSY-like multiplet pattern due to scalar couplings to the passive $^{13}C^\beta$ spin. The wealth of correlations encountered in some spectral regions can however obstruct the evaluation of relevant cross peaks to a higher extent than in triple-resonance E.COSY methods where only one or two signals per

*To whom correspondence should be addressed.

residue are detected. While it is conceivable to remove this overlap in a 4D ^{15}N,^{13}C-separated NOESY experiment, it may be difficult to achieve an adequate resolution for the ^3J determination.

In this paper we describe an experimental scheme capable of measuring either $^3J(C'_{i-1},C^{\beta}_i)$ or $^3J(H^N_i,C^{\beta}_i)$ coupling constants in isotopically labelled proteins independent of the residue type and the magnitude of the couplings themselves. It is based on the well-known HNCACB pulse sequence (Wittekind and Mueller, 1993) and correlates amide protons and nitrogens with β-carbons of the same and the preceding residue. Depending on whether $^{13}C'$ or $^1H^N$ spins are left untouched during the ^{15}N evolution period, intraresidual E.COSY-like multiplets arise from which either of the two vicinal coupling constants can be determined in the indirectly detected $^{13}C^{\beta}$ dimension. Interchanging active and passive spins compared to the E.COSY experiments mentioned above abandons the need to discriminate between α- and β-carbons by bandselective pulses.

A different approach for the determination of $^3J(H^N_i,C^{\beta}_i)$ has already been proposed but not demonstrated by Seip et al. (1994). The direct scalar correlation of nitrogens and β-protons via long-range couplings using the HNHB scheme (Archer et al., 1991) yields H^N-H^{β} cross peaks, where the doublet components corresponding to the different $^{13}C^{\beta}$ spin states are displaced by $^1J(H^{\beta},C^{\beta})$ and $^3J(H^N,C^{\beta})$ in orthogonal dimensions. Since carbon nuclei are not needed for any magnetization transfer step, no perturbation of the passive $^{13}C^{\beta}$ spins can occur. Here, we report the succesful implementation of the HNHB[C^{β}]-E.COSY experiment (according to the nomenclature of Wang and Bax (1995) the nucleus to which the J coupling is measured is indicated by the square brackets).

Materials and methods

Description of pulse sequences

In contrast to the original HNCACB sequence, all 90° and 180° carbon pulses in the $^{13}C'$-coupled version diagrammed in Figure 1A selectively cover the aliphatic region, ensuring that the $^{13}C'$ spin states are not disturbed during t_1 or t_2. Carbonyl decoupling during acquisition is on the other hand mandatory here, because otherwise the multiplet components corresponding to the $^{13}C'$ α and β spin states would not only be separated by $^1J(N,C')$ in F1 and by $^3J(C',C^{\beta})$ in F2 but additionally be displaced by $^2J(H^N,C')$ in the F3 dimension, leading to an undesired tilt. Sensitivity enhancement combined with gradient coherence selection in the final reverse INEPT step is accomplished in the usual manner (Palmer et al., 1991; Kay et al., 1992). During the preparation of the manuscript a conceptionally identical experiment for the measurement of $^3J(C',C^{\beta})$, named [CO]HN(CA)CB-E.COSY, was published by Hu and Bax (1998). Some minor differences are however worth mentioning and shall be briefly described in the following.

In order to resolve the ^{15}N-$^{13}C'$ splitting a relatively long ^{15}N evolution period is required. Therefore, the magnetization transfer from the amide nitrogens to α-carbons is implemented in an HMQC manner rather than by use of INEPT steps, allowing to exploit both the de- and rephasing delays for ^{15}N constant time chemical shift evolution (Madsen and Sørensen, 1992). If the chosen constant time delay T_N exceeds twice the optimal intraresidual ^{15}N-$^{13}C^{\alpha}$ transfer time T (≈ 31 ms for averaged $^1J(N,C^{\alpha})$ and $^2J(N,C^{\alpha})$ coupling constants of 10.5 and 7.5 Hz, respectively (Delaglio et al., 1991)), a delay $\zeta = T_N/4 - T/2$ has to be inserted between the 180° pulses on ^{15}N and $^{13}C^{\alpha}$. As a possible simplification of the ct-^{15}N evolution period, the second 180° pulse on nitrogens may be omitted in combination with a reversal of the direction in which the first ^{15}N refocussing pulse is shifted. In order to use the entire T_N period for ^{15}N evolution, the first G3 pulse on α-carbons would then be applied at a time ζ after the associated nitrogen pulse. However, for the ease of pulse programming, the version of Figure 1A avoids a crossing of any pulse with the start of ^{1}H decoupling.

While the sequence by Hu and Bax (1998) employed a constant time $^{13}C^{\beta}$ evolution period adjusted to $1/^1J(C^{\alpha},C^{\beta})$, we prefer a non-constant time t_2 period to maximize integrated signal intensities and to avoid a restriction of the resolution in the domain in which the coupling of interest is determined. On the other hand, undesired one-bond carbon-carbon couplings evolve during t_2 in our variant, leading to additional multiplet splittings at the expense of the signal-to-noise ratio. Finally, care has been taken in the present implementation to prevent any dephasing of the water magnetization by the action of the B_0 field gradients (Grzesiek and Bax, 1993; Stonehouse et al., 1994) or by RF inhomogeneity during proton composite-pulse decoupling (Kay et al., 1994) such that no saturation of rapidly exchanging amide protons occurs.

The HNCACB[H^N]-E.COSY pulse sequence outlined in Figure 1B employs the same magnetization

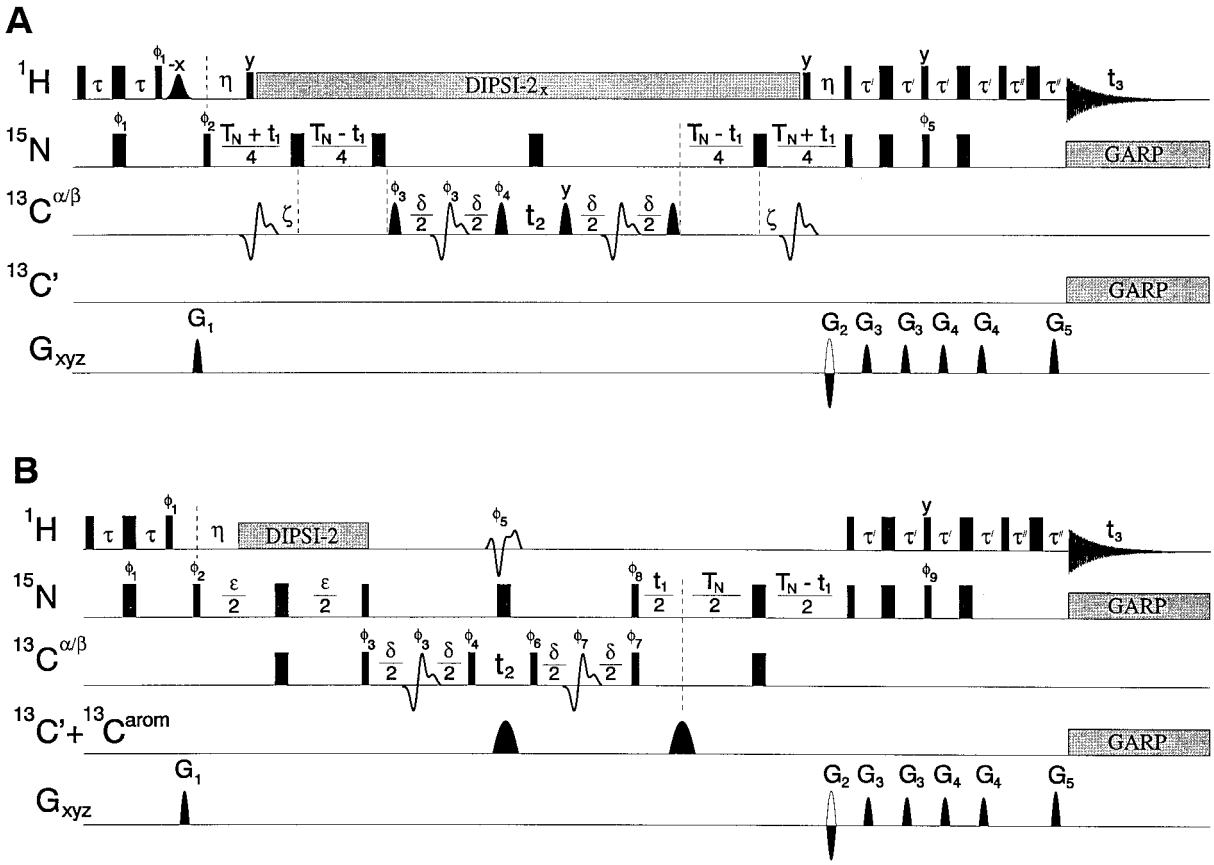

Figure 1. HNCACB-E.COSY pulse schemes for the measurement of (A) $^3J(C'_{i-1},C_i^{\beta})$ and (B) $^3J(H_i^N,C_i^{\beta})$ coupling constants. Narrow and wide filled bars denote rectangular pulses with 90° and 180° flip angles, respectively. Unless indicated explicitly, pulse phases are adjusted to the +x axis. The proton carrier frequency is placed onto the H_2O resonance throughout sequence A, while it is temporarily switched to 8.54 ppm for the duration of the DIPSI-2 (Shaka et al., 1988) decoupling sequence (4.5 kHz RF field) and to 2.67 ppm during the 1.59 ms I-BURP-1 (Geen and Freeman, 1991) pulse in the centre of t_2 in version B. The water-selective 90° pulse with phase −x in version A has a Gaussian shape and a duration of 2.5 ms. In each sequence the first and last carbon pulses are shifted to 58 ppm by phase modulation, the carbon carrier being positioned at 46.25 ppm. The widths of rectangular carbon pulses are adjusted to provide a null in their excitation profile in the carbonyl region while the refocusing pulse centered in the delays δ are 250 μs G3 Gaussian cascades (Emsley and Bodenhausen, 1990). The G3 inversion pulses applied in the T_N period of sequence A have a width of 500 μs. Bandselective 90° pulses on aliphatic carbons have the shape of the centre lobe of a sinc function and a width of 90 μs. Refocusing of scalar couplings involving carbonyl or aromatic γ-carbons during both evolution times of sequence B is accomplished by 200 μs cosine-modulated 180° sinc-pulses with two excitation maxima at 176 and 133.5 ppm. GARP-1 modulation (Shaka et al., 1985) with RF fields of 1 kHz and 0.75 kHz, respectively, is employed for $^{13}C'$ and ^{15}N decoupling during acquisition. All gradients are sine-bell shaped and have the following durations, strengths at their centre and directions: G_1: 0.7 ms, 10 G cm^{-1} (y); G_2: 1 ms, −39.4/39.4 G cm^{-1} (z); G_3: 0.5 ms, 4 G cm^{-1} (x), 5.5 G cm^{-1} (y); G_4: 0.5 ms, 5.5 G cm^{-1} (x), 4 G cm^{-1} (y); G_5: 0.5 ms, 8 G cm^{-1} (z). For each t_1 increment N- and P-type signals are collected alternately by inverting the polarity of G_2 along with the pulse phases ϕ_5 (A) or ϕ_9 (B). After each t_1 increment the pulse phases ϕ_2 (A) or ϕ_8 (B) are inverted together with the receiver reference phase. Quadrature detection in the t_2 dimension is achieved by applying the States-TPPI protocol (Marion et al., 1989a) to phases ϕ_3 and ϕ_4. Delay durations are adjusted as follows: $\tau = 2.3$ ms, $\eta = 5.4$ ms, $\epsilon = 29$ ms, $\zeta = 2.1$ ms, $\delta = 13.4$ or 9.6 ms, $\tau' = 2.5$ ms, $\tau'' = 0.7$ ms. The lengths of the constant-time evolution periods T_N are 70.4 and 26.5 ms in versions A and B, respectively. Phase cycles are: (A) ϕ_1 = y, −y, ϕ_2 = 2(x), 2(−x), ϕ_3 = 4(x), 4(−x), ϕ_4 = 2(y), 2(−y), ϕ_5 = y, Rec. = x, 2(−x), x, −x, 2(x), −x and (B) ϕ_1 = y, −y, ϕ_2 = 2(x), 2(−x), ϕ_3 = 4(x), 4(−x), ϕ_4 = 2(y), 2(−y), ϕ_5 = 8(x), 8(−x), ϕ_6 = y + 45°, ϕ_7 = x + 45°, ϕ_8 = x, ϕ_9 = y, Rec. = x, 2(−x), x, −x, 2(x), −x. Phases ϕ_6 and ϕ_7 are adjusted to compensate for zero-order Bloch–Siegert errors, as indicated.

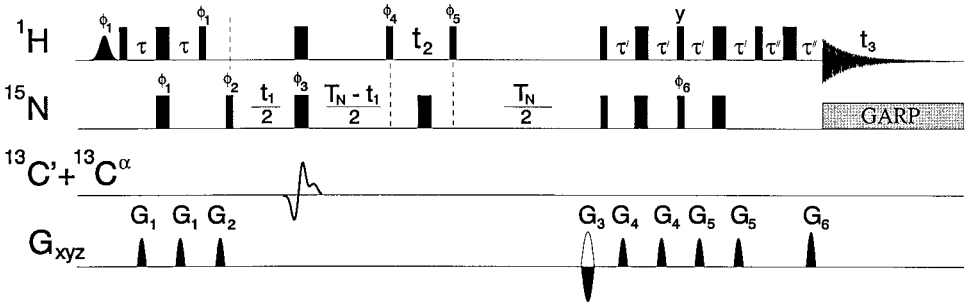

Figure 2. HNHB[C^{β}]-E.COSY experiment for measuring $^{3}J(H_i^N,C_i^{\beta})$ coupling constants. The initial water selective 90° Gaussian pulse has a duration of 10 ms. All further pulses applied to proton and nitrogen spins are rectangular, employing RF fields of 17 and 7 kHz, respectively. Nitrogen decoupling is achieved by a 0.96 kHz GARP-1 modulation. The 180° carbon pulse, centered at 116 ppm has a G3 envelope with a duration of 500 μs. A simultaneous inversion of carbonyl and α-carbon spins is accomplished via appropriate cosine modulation. The delays τ, τ′ and τ″ are set to 2.3 ms, 2.5 ms and 0.7 ms, respectively. T_N is adjusted to either 75.6 or 96.4 ms. Gradients and phase cycling: G_1: 1 ms, 7.5 G cm^{-1} (x); G_2: 1 ms, 10 G cm^{-1} (y); G_3: 1 ms, −39.4/39.4 G cm^{-1} (z); G_4: 0.7 ms, 4 G cm^{-1} (x), 5 G cm^{-1} (y); G_5: 0.7 ms, 5 G cm^{-1} (x), 4 G cm^{-1} (y); G_6: 0.5 ms, 8 G cm^{-1} (z); ϕ_1 = y, −y, ϕ_2 = 2(x), 2(−x), ϕ_3 = 8(x), 8(y), ϕ_4 = 4(x − 45°), 4(−x − 45°), ϕ_5 = 8(x), 8(−x), ϕ_6 = y, Rec. = x, 2(−x), x, −x, 2(x), −x. Echo- and antiecho coherence transfer pathways in t_1 are selected alternately by concerted sign reversal of G_3 and ϕ_6. The phase ϕ_4 is changed in the TPPI manner (Marion and Wüthrich, 1983) to achieve quadrature detection in t_2.

transfer pathway as the previous one except for the polarization transfer steps from ^{15}N to $^{13}C^{\alpha}$ and vice versa which now replace the HMQC-type element. The most important difference, however, is that amide proton decoupling is not extended over the t_1 and t_2 evolution times. As a consequence, the $^{1}J(H^N,N)$ and $^{3}J(H^N,C^{\beta})$ couplings give rise to an E.COSY multiplet pattern in the F1,F2 plane of the 3D spectra with an antiphase doublet structure along the ^{15}N dimension. The large $^{13}C^{\beta}$-$^{1}H^{\beta}$ splitting is eliminated by an I-BURP pulse (Geen and Freeman, 1991) applied in the centre of t_2, selectively inverting the $^{1}H^{\beta}$ region while leaving amide protons untouched. Refocusing of $^{1}J(C^{\beta},C^{\gamma})$ couplings in aromatic and Asx side chains is achieved by a 200 μs cosine-modulated sinc-shaped 180° pulse with its two excitation maxima set to the centre of the carbonyl and the aromatic carbon regions. Carbonyl decoupling during acquisition is optional here, but is is recommended as it results in a slight line-narrowing through removal of ^{2}J and ^{3}J $^{1}H^N$-$^{13}C'$ interactions.

The HNHB[C^{β}]-E.COSY pulse sequence (Figure 2) is based on the HNHB version of Madsen et al. (1993), including a ^{15}N full-sweep constant time evolution period and the sensitivity enhancement scheme combined with gradient coherence selection. When applied to a doubly labelled protein passive scalar interactions involving $^{13}C^{\beta}$ spins occur in both proton dimensions, enabling the $^{3}J(H^N,C^{\beta})$ coupling constants to be measured from $^{1}H^{\beta}$(F2)-$^{1}H^N$(F3) cross peaks. The only carbon pulse which has to be introduced inverts $^{13}C'$ and $^{13}C^{\alpha}$ magnetization in order to remove one-bond and two-bond splittings in the ^{15}N dimension. Being applied before the start of the t_2 evolution time for any value of t_1, it does not affect the E.COSY-like multiplet pattern. A further modification involves the enhancement of signals from fast exchanging amide protons by the constructive use of radiation damping. In more detail, the initial water-selective pulse, together with the 90° hard pulse of the same phase (ϕ_1) aligns the H_2O magnetization along the −z axis before the application of the purge gradient G_2. A relatively high selectivity could be achieved by the shaped proton pulse without any sensitivity loss due to relaxation as it acts before the excitation of protein resonances (Matsuo et al., 1996; Andersson et al., 1998). The water magnetization is then flipped back to +z by the following 180° pulse and adopts different orientations depending on the phase relation of the two 90° pulses flanking the t_2 evolution period. However, as demonstrated by Jahnke et al. (1995), a displacement by 45° results in a constant magnitude of the transverse component for all steps of the TPPI cycling employed for ω_2 frequency discrimination such that the radiation damping field always brings the water back to the +z axis prior to the phase-encoding gradient G_3. The overall effect of the remaining proton pulses on the H_2O magnetization is merely a 720° rotation around the x-axis and therefore no dephasing occurs by the final gradient, avoiding a saturation of exchangeable amide protons.

NMR measurements

All pulse sequences have been applied to recombinant $^{13}C/^{15}N$-labelled *Desulfovibrio vulgaris* flavodoxin (MW = 16.3 kDa at natural isotopic abundance). A 1.4 mM protein sample dissolved in 95% H_2O/5% D_2O, 10 mM KPi (pH = 7.0) was used. The temperature was set to 27 °C. HNCACB-E.COSY and HNHB-E.COSY experiments were carried out at ^1H resonance frequencies of 600 and 800 MHz, respectively, using Bruker Avance spectrometers equipped with 5 mm three-axis gradient $^1H\{^{13}C,^{15}N\}$ triple resonance probes.

In the HNCACB-E.COSY experiments the duration of the δ delay for the polarization transfer between $^{13}C^{\alpha}$ and $^{13}C^{\beta}$ was empirically optimized for $^{13}C^{\beta}$ signal intensity, yielding a value of 9.6 ms for flavodoxin. Cross peaks involving α-carbons can however be cancelled by adjusting δ to $1/(2\ ^1J(C^{\alpha},C^{\beta}))$, thus eliminating a potential source of overlap. Therefore, each of the two variants was recorded twice with δ values of either 9.6 or 13.4 ms. Spectral widths were 14.7, 20.0 and 15.1 ppm in the ^{15}N, ^{13}C, and $^1H^N$ domains, respectively. The data sets consisted of 64 (t_1, ^{15}N) × 127 (t_2, ^{13}C) × 896 (t_3, $^1H^N$) complex points for the $^{13}C'$-coupled version (A) and 22 (t_1, ^{15}N) × 152 (t_2, ^{13}C) × 896 (t_3, $^1H^N$) complex points for the $^1H^N$-coupled version (B), corresponding to acquisition times of, respectively, 70.4 ms, 42.1 ms, 99 ms (t_1, t_2, t_3) and 23.5 ms, 50.4 ms, 99 ms (t_1, t_2, t_3). For each FID, eight scans were accumulated in version A (measuring time: 86 h) while 16 scans were collected in version B (measuring time: 73 h). In addition, a pair of HNCACB[C′]-E.COSY data sets (δ = 9.6 ms and δ = 13.4 ms) was recorded with a prolonged ^{13}C acquisition time of 61.6 ms (186 t_2 increments) and a shortened relaxation delay, otherwise using identical parameters as above (measuring time: 99 h).

The HNHB[C^{β}]-E.COSY experiment was carried out twice with the delay $T_N/2$ for the evolution of ^{15}N-^1H couplings adjusted to either 48.2 ms ($\approx 9[2^1J_{NH}]^{-1}$) or 37.8 ms ($\approx 7[2^1J_{NH}]^{-1}$). Spectral widths comprised 15.0 ppm in F3 ($^1H^N$), 21.2 ppm in F1 (^{15}N) and 8.2 ppm in F2 (^1H). Acquisition times were 85.3 ms in t_3 (1024 complex points), 20.9 ms in t_1 (36 complex points) and 16.9 ms in t_2 (222 real points). Accumulation of 16 scans per FID resulted in a recording time of 80 h for each of the two spectra.

Processing and evaluation of spectra

Spectra were processed with Felix 1.1 (Hare Research, Inc., Woodinville, WA, USA). In all experiments, time domain data were extended by mirror-image linear prediction (Zhu and Bax, 1990) in the ^{15}N dimension, while backward linear prediction of the first points was applied in the $^{13}C^{\beta}$ and $^1H^{\beta}$ dimensions of the HNCACB- and HNHB-E.COSY spectra, respectively, to avoid a first order phase correction. Apodization in the HNCACB-E.COSY data sets involved multiplication with a squared cosine-bell in the ^{13}C and $^1H^N$ dimensions and a squared sine-bell, shifted by 60°, in the ^{15}N dimension. A squared cosine-bell multiplication was applied in all three dimensions of the HNHB-E.COSY. The residual H_2O signal was eliminated in all spectra by time domain deconvolution along t_3 (Marion et al., 1989b). After zero-filling and Fourier transformation the digital resolution in the dimensions relevant for the measurement of the ^3J couplings was 5.9 Hz in both the HNCACB- and HNHB-E.COSY data sets.

Vicinal coupling constants were extracted from the horizontal displacement of the upper and lower multiplet components by a trace-alignment procedure. The two F2 (F3) traces in the HNCACB-E.COSY (HNHB-E.COSY) spectra were generated by summing over appropriate points in the F1 and F3 (F1 and F2) dimensions and were then inversely Fourier transformed and subjected to a least-squares superposition in the time domain (Schmidt et al., 1995).

Results and discussion

The pulse sequences proposed here are suitable for the measurement of ϕ-related vicinal coupling constants involving $^{13}C^{\beta}$ for all amino acid residue types except for proline (and glycine, of course). This contrasts with E.COSY methods relying on $^1J(C^{\alpha},C^{\beta})$ to separate the multiplet components corresponding to the two passive spin states which certainly fail for serines and threonines and possibly also for leucine and aromatic residues with downfield shifted $^{13}C^{\beta}$ resonances. Typical intraresidual cross peaks from both types of HNCACB-E.COSY spectra are shown in Figures 3 and 4. Apparently, the optimal superposition of the projected F1 doublet components is not affected by the relatively low digital resolution in F2 as the alignments were carried out in the time domain. Vertical splittings correspond to $^1J_{NC'}$ and $^1J_{NH}$ couplings, respectively, while partially resolved doublet, triplet or quadruplet fine structures appear along F2, depending on the number of ^{13}C spins directly bound to the respective β-carbons. Their one-bond

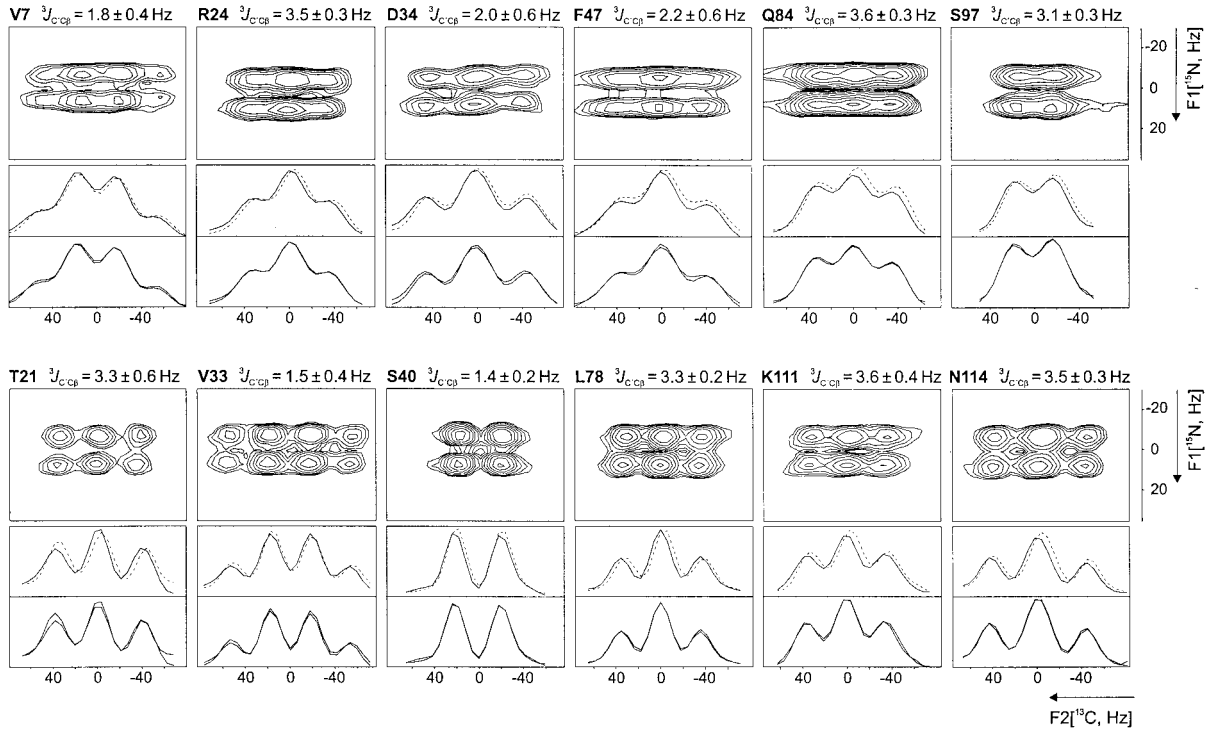

Figure 3. Determination of $^3J(C'_{i-1},C^{\beta}_{i})$ coupling constants in *Desulfovibrio vulgaris* flavodoxin from 3D HNCACB[C′]-E.COSY spectra recorded with ^{13}C (F2) acquisition times of 42.1 ms (upper row) and 61.6 ms (lower row). The contour plots show cross sections through ^{15}N(F1)-$^{13}C^{\beta}$(F2) signals taken at the intraresidual $^1H^N$ resonance positions of the residues given at the top. One-dimensional projections of the high-field (dashed line) and low-field (solid line) multiplet halves are obtained by summing over appropriate spectral points in F1 and F3. A superposition of traces after fitting their amplitude and horizontal positions is shown at the bottom of each panel. Different numbers of F2 data points were included to account for the varying multiplet widths. Measured *J* values are indicated together with the uncertainty of the fitted horizontal displacements.

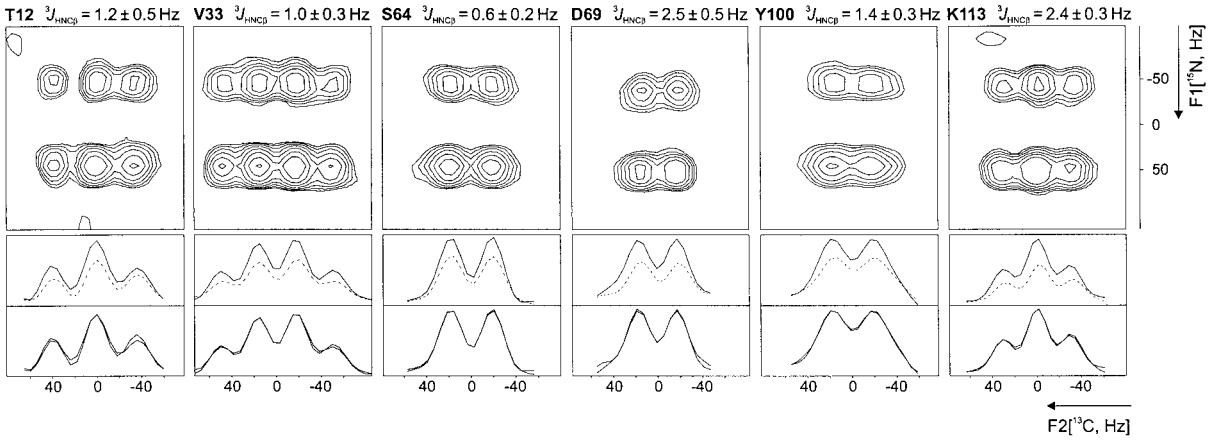

Figure 4. Extraction of $^3J(H^N_i,C^{\beta}_{i})$ coupling constants from intraresidual cross peaks in HNCACB[H^N]-E.COSY spectra of flavodoxin. Multiplets exhibit an antiphase splitting in the ^{15}N domain owing to the coupling to the directly bound protons. Positive and negative contours are drawn without distinction. For clarity, the projection of the negative upper multiplet half (dashed line) has been inverted. Its intensity is scaled up during the time-domain trace alignment procedure, the result of which is shown at the bottom.

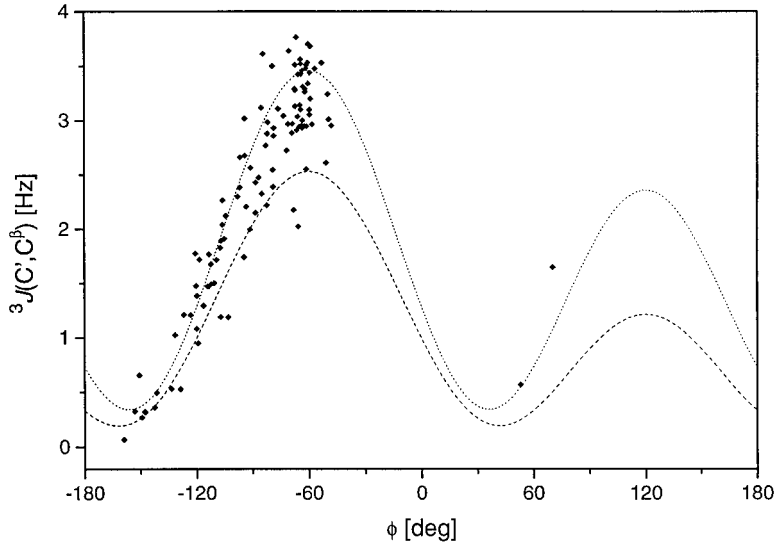

Figure 5. Dependence of HNCACB-E.COSY-derived $^3J(C'_{i-1},C^\beta_i)$ coupling constants in oxidized *Desulfovibrio vulgaris* flavodoxin on the ϕ-torsional angles in its crystal structure (M. Walsh, unpublished results). The dotted and dashed lines are Karplus parametrizations taken from Löhr et al. (1997) and from Hu and Bax (1997), respectively.

interaction with γ-carbons in Asp/Asn and aromatic residues can be eliminated in the H^N- but not in the CO-coupled version. In the latter, therefore, a distortion occurs in the ^{15}N dimension due to the χ^1-dependent intraresidual $^3J(N,C^\gamma)$ coupling, which may lead to an increased uncertainty in the determination of $^3J(C'_{i-1},C^\beta_i)$ from the displacement along the orthogonal $^{13}C^\beta$ domain (see, e.g., D34 in Figure 3). Contrary to the C^β-constant time version (Hu and Bax, 1998) the size of the $^3J(N,C^\gamma)$ coupling constants in these residues cannot be measured here along F1, because the $^1J(C^\beta,C^\gamma)$ splitting is not completely resolved. In the HNCACB[H^N]-E.COSY (Figure 4) ^{15}N high-field and low-field doublet components have clearly unequal intensities. This effect arises from differential relaxation caused by ^{15}N CSA/^1H-^{15}N dipole cross-correlation (Goldman, 1984; Tjandra et al., 1996) during the constant time evolution period T_N. It does not interfere with the evaluation of vicinal coupling constants as the amplitudes are fitted together with the horizontal displacements during the trace alignment procedure.

As demonstrated in Figure 3, the precision in the determination of coupling constants can be slightly improved by increasing the resolution. However, this can only be achieved at the expense of a longer recording time because they are measured in an indirectly detected dimension. In any case, the most important limitation is the relatively fast transverse relaxation of the $^{13}C^\beta$ coherences.

Analysis of the HNCACB-E.COSY spectra yielded a total of 112 $^3J(C',C^\beta)$ and 86 $^3J(H^N,C^\beta)$ values for the 126 non-glycine and non-proline residues of flavodoxin. The smaller number of $^3J(H^N,C^\beta)$ coupling constants is due to increased spectral overlap as a consequence of the larger one-bond coupling and the lower resolution in the ^{15}N domain. A remedy for this problem would be the introduction of a spin-state-selective excitation (S^3E) element (Meissner et al., 1997a,b, 1998a) prior to the ^{15}N evolution time in the pulse sequence of Figure 1B, allowing for the decoupling of $^1J_{NH}$ during t_1.

Multiple determination of the coupling constants in different spectra of the same type permitted the assessment of their random errors. The pairwise rms differences in the *J* values were 0.67 and 0.63 Hz in the $^{13}C'$- and $^1H^N$-coupled HNCACB-E.COSY versions, respectively. In Figure 5, the average values for $^3J(C',C^\beta)$ are plotted versus the ϕ-torsion angles derived from the flavodoxin 1.7 Å X-ray structure (M. Walsh, unpublished results). Two empirical Karplus curves based on protein data are also shown in Figure 5. The curve of Hu and Bax (1997) resulted from the application of the HN(CO)C quantitative *J* correlation method to human ubiquitin, while the parametrization of Löhr et al. (1997) has been carried out with flavodoxin using an H(N)CA,CO[C^β]-E.COSY

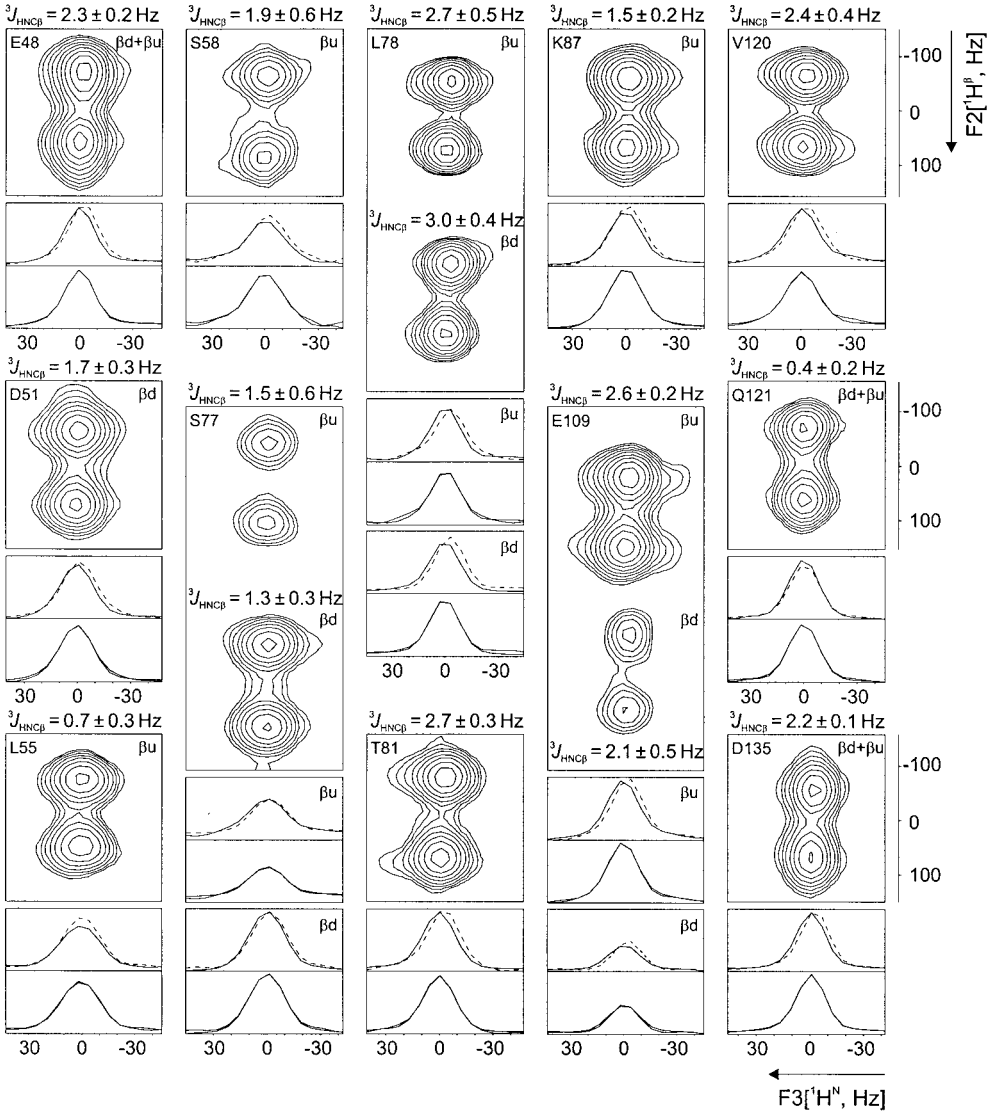

Figure 6. Representative cross peaks from a 3D HNHB[C^{β}]- E.COSY spectrum of flavodoxin. Projections of the two major multiplet components before and after trace alignment along F3 are shown in the lower half of each panel. The resulting $^{3}J(H_i^N,C_i^{\beta})$ coupling constants are indicated. βd and βu denote the downfield and upfield β-methylene ^{1}H resonances, respectively. For residues S77, L78 and E109 vicinal coupling constants can be measured separately from both cross peaks while in E48, Q121 and D135 the two β-protons are degenerate.

experiment. Overall the coupling constants obtained in this study fit better to the flavodoxin curve, the average values being only slightly smaller than predicted by the latter. The decrease may be explained by the passive spin flips occurring during the two δ periods and the $^{13}C^{\beta}$ (t_2) evolution time, although the influence on the relative displacement of the multiplet components is expected to be small considering the relatively long carbonyl T_1 relaxation times (Hu and Bax, 1998). Note that in the H(N)CA,CO-E.COSY pulse sequence this effect was minimized owing to the immediate consecution of t_1 and t_2. In contrast, a larger systematic error towards lower *J* values occurs in the H^N-coupled version of the HNCACB-E.COSY. At 600 MHz, selective $^{1}H^N$ T_1 values for flavodoxin fall in the 0.12–0.2 s range (F. Löhr and H. Rüterjans, unpublished results), leading to an underestimation of $^{3}J(H^N,C^{\beta})$ of up to approximately 10%. As pointed out recently (Meissner et al., 1998b), this source of error could be eliminated in an S^3E E.COSY version

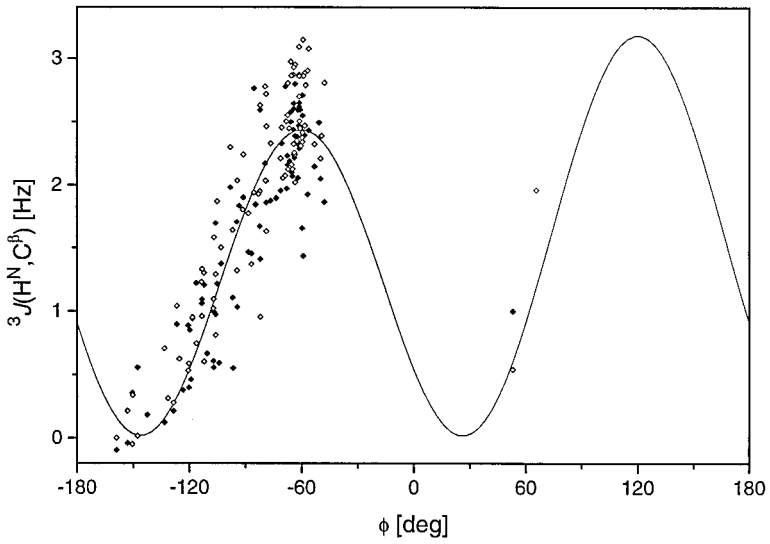

Figure 7. Relation between $^3J(H_i^N,C_i^\beta)$ coupling constants measured for oxidized *Desulfovibrio vulgaris* flavodoxin and its crystal structure-derived ϕ-angles. Filled and open diamonds represent the average values obtained from the two HNCACB[H^N]-E.COSY and the two HNHB[C^β]-E.COSY spectra, respectively. The solid line is the Karplus curve parametrized with the X-ray structure of human ubiquitin (Wang and Bax, 1996).

of the pulse sequence, but it was not attempted here as the random variation of the coupling constants appears to be larger in our measurements.

As an alternative to the HNCACB[H^N]-E.COSY, $^3J(H^N,C^\beta)$ coupling constants can be measured by the HNHB[C^β]-E.COSY method. The latter is a relatively simple experiment which does not require extensive optimization. The coupling of interest is detected in the directly acquired dimension, allowing an adjustment of the resolution in this domain without taking the total recording time into account. The signal-to-noise ratio is not degraded by one-bond carbon-carbon splittings as in the HNCACB-E.COSY experiments. On the other hand, the transfer efficiency in the HNHB depends on long range interactions (i.e. $^3J(N,H^\beta)$) which may be vanishingly small. A further drawback is that for β-CH_2 groups overlap can be introduced by the appearance of cross peaks involving both $^1H^\beta$ nuclei. For these reasons the HNHB[C^β]-E.COSY experiments were carried out at 800 MHz, gaining the highest possible sensitivity and spectral resolution. Again, the resolution might be further improved by decoupling of $^1J(H^\beta,C^\beta)$ in t_2 using an S^3E element.

Examples of cross peaks from the HNHB[C^β]-E.COSY spectra are given in Figure 6. In a few amino acid residues in flavodoxin (e.g. S77, L78 and E109) the pair of β-methylene signals is well separated and of sufficient intensity to extract the $^3J(H^N,C^\beta)$ coupling constants from both cross peaks. The discrepancy between the two values simply reflects the random error of the ^3J measurement. A degeneracy of the two $^1H^\beta$ resonances can be advantageous in this experiment, because it increases the signal-to-noise ratio while not preventing an evaluation of the E.COSY peaks – contrary to the case where the chemical shifts are not identical, but differ by less than the one-bond C^β,H^β splitting plus two times the H^β linewidth. The two HNHB[C^β]-E.COSY spectra recorded for flavodoxin yielded $^3J(H^N,C^\beta)$ coupling constants for 89 residues with a pairwise rms difference of 0.47 Hz.

Since one of the three dimensions differs between the HNCACB[H^N]-E.COSY and HNHB[C^β]-E.COSY spectra the two experiments complement each other with respect to signal overlap. Altogether, therefore, $^3J(H^N,C^\beta)$ values are available for a considerable fraction (109 out of 126 potential) of the residues in flavodoxin. Their dependence on the crystal structure-derived ϕ-angles is depicted in Figure 7. In contrast to our $^3J(C',C^\beta)$ data, the $^3J(H^N,C^\beta)$ coupling constants from both types of measurements do not seem to deviate systematically from the ubiquitin-derived Karplus curve (Wang and Bax, 1996). On average, larger couplings were observed in the HNHB[C^β]-E.COSY experiment than in the HNCACB[H^N]-E.COSY. We presume that this effect is caused by the longer lifetime of the passive $^{13}C^\beta$

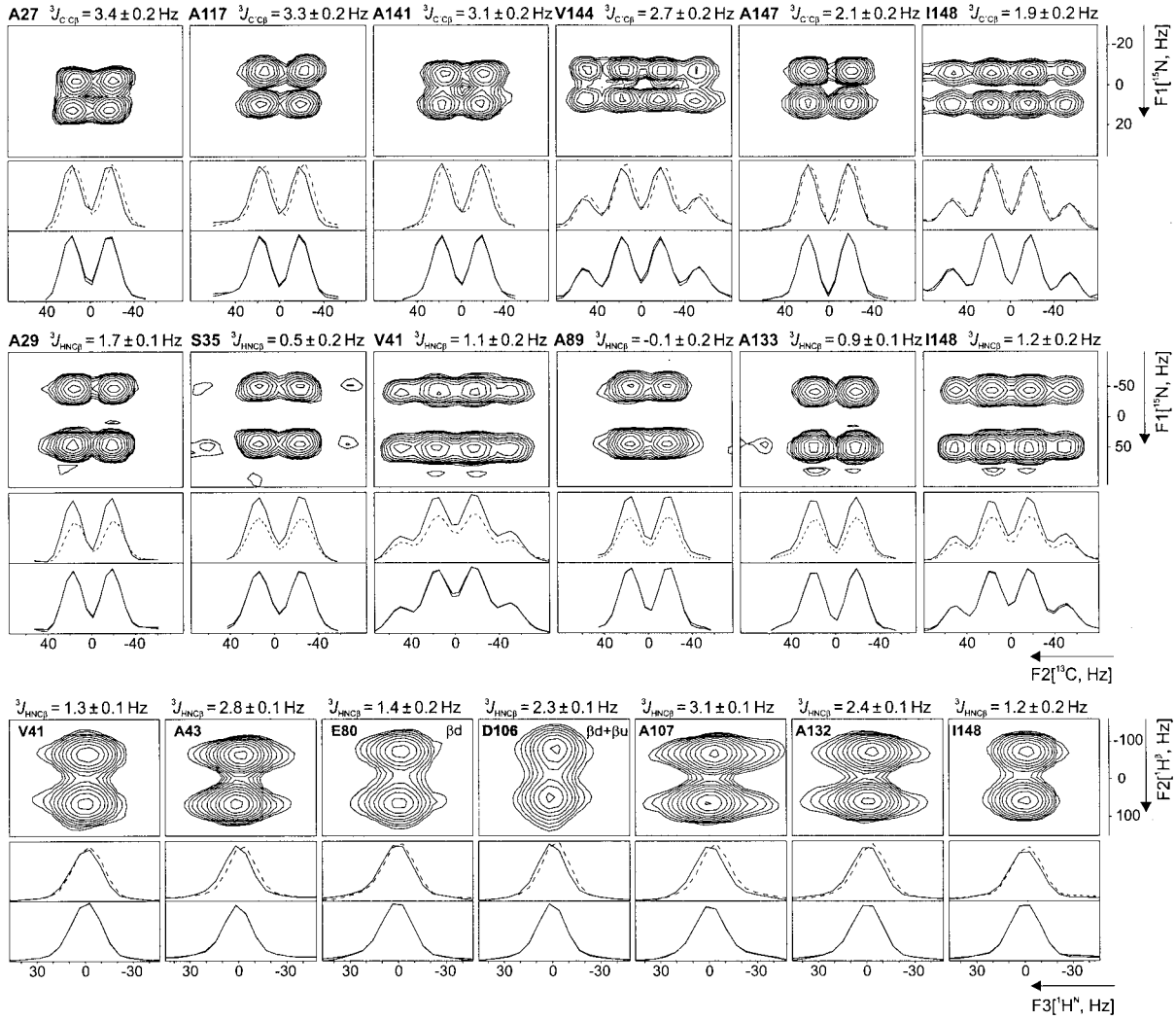

Figure 8. Measurement of $^3J(C'_{i-1},C^{\beta}_i)$ and $^3J(H^N_i,C^{\beta}_i)$ for selected residues of flavodoxin. The cross peaks were chosen on the basis of their above-average signal-to-noise ratios and the correspondingly small uncertainty of the trace alignment procedure. The first, second and third row show examples from HNCACB[C′]-E.COSY, HNCACB[H^N]-E.COSY and HNHB[C^{β}]-E.COSY spectra, respectively.

spin states compared to $^1H^N$. This explanation is substantiated by the fact that the majority of the values around 3 Hz were measured for alanine residues, which exhibit the longest $^{13}C^{\beta}$ T_1 relaxation times in a protein.

The experimental data presented in Figures 5 and 7 show a large scattering of both types of vicinal couplings around the maxima of the Karplus curves at $-60°$ in particular, and discrepancies to the back-calculated values of up to approximately 1 Hz are observed. This may not only be caused by differences between the backbone conformations of flavodoxin in the crystal and in solution, as only minor deviations from its X-ray structure (Watt et al., 1991) were detected by NMR (Stockman et al., 1994; Knauf et al., 1996; Blümel et al., 1998), but rather has to be primarily attributed to random experimental errors. However, a variation of the motional averaging along the protein backbone may also contribute to the spread of ^3J coupling constants for similar crystallographic torsion angles (Hoch et al., 1985; Brüschweiler and Case, 1994).

The inherently low sensitivity of both the HNCACB- and HNHB-E.COSY methods led to a relatively high uncertainty of the measured ^3J values for a number of residues, which is reflected in a poor fit

of the two multiplet components after trace alignment as well as in large variations upon repeated measurements. Good signal-to-noise ratios were however obtained for the 17 alanine residues in flavodoxin owing to their reduced $^1H^{\beta}/^{13}C^{\beta}$ linewidths. A further contribution, which is particularly important for the HNCACB-E.COSY experiments, is the presence of only one homonuclear coupling partner, while in the case of the HNHB[C^{β}]-E.COSY the intensity is increased through the superposition of cross peaks from three equivalent β-protons. As a result, $^3J(C',C^{\beta})$ and $^3J(H^N,C^{\beta})$ couplings can be determined with a relatively high precision. This is demonstrated in Figure 8 for several alanines as well as a few other residues in flavodoxin that exhibit increased mobility and therefore diminished transverse relaxation rates (e.g. the C-terminal I148). Note that in addition the cross peak intensity for non-alanine residues is conformation dependent in the HNHB-E.COSY because of the magnetization transfer via $^3J(N,H^{\beta})$. Within a group of 23 residues in flavodoxin comprising all alanines and residues S35, V41, E80, D106, V144, I148, pairwise rms differences for the coupling constants measured in the HNCACB[C′]-E.COSY, the HNCACB[H^N]-E.COSY and the HNHB[C^{β}]-E.COSY were reduced to 0.48, 0.31 and 0.24 Hz, respectively. As shown in Figure 9 the coupling data for this group agrees reasonably well with the values expected from the conformation in the X-ray structure. This implies that, depending on the sensitivity that can be achieved, the methods proposed here are able to provide useful information to complement other ^3J data for a more accurate determination of backbone torsion angles ϕ in proteins.

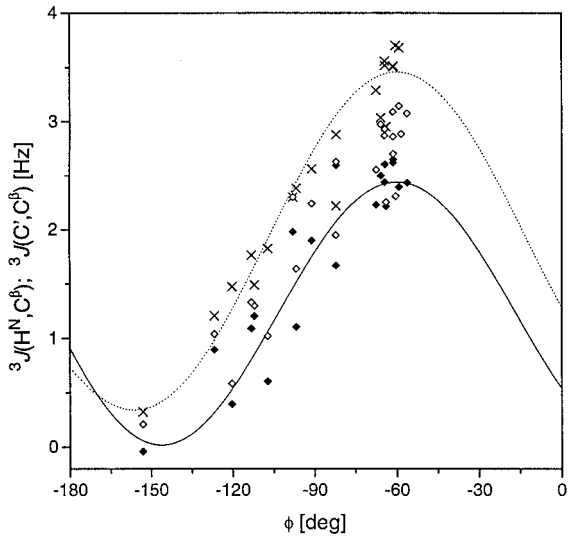

Figure 9. Subset of the coupling data presented in Figures 5 and 7. Average $^3J(C'_{i-1},C^{\beta}_i)$ coupling constants from HNCACB[C′]-E.COSY spectra (crosses) and $^3J(H^N_i,C^{\beta}_i)$ coupling constants from HNCACB[H^N]-E.COSY (filled diamonds) and HNHB[C^{β}]-E.COSY (open diamonds) spectra are plotted versus the ϕ-angles of 17 alanine residues as well as S35, V41, E80, D106, V144 and I148 in the flavodoxin crystal structure. Solid and dotted lines are Karplus curves represented by $^3J(H^N_i,C^{\beta}_i) = 2.78\cos^2(\phi + 60°) - 0.37\cos(\phi + 60°) + 0.03$ Hz (Wang and Bax, 1996) and $^3J(C'_{i-1},C^{\beta}_i) = 2.54\cos^2(\phi - 120°) - 0.55\cos(\phi - 120°) + 0.37$ Hz (Löhr et al., 1997), respectively.

Conclusions

Pulse sequences have been introduced for the determination of two ϕ-angle-related vicinal coupling constants. The underlying E.COSY principle ensures that arbitrarily small interactions can be detected while the choice of the passive spins allows their application for all relevant residue types. Due to sensitivity limitations less precise values were obtained for flavodoxin when compared to previously published E.COSY experiments. It has been demonstrated, however, that a reliable measurement of $^3J(C',C^{\beta})$ and $^3J(H^N,C^{\beta})$ should be feasible for small proteins with favourable relaxation properties. Alternatively, the two versions of the HNCACB-E.COSY sequence can be applied to $^2H/^{13}C/^{15}N$-labelled proteins after slight modifications to include deuterium decoupling, benefitting from the markedly prolonged $^{13}C^{\alpha/\beta}$ T_2 relaxation times. Therefore, in cases where the sensitivity losses arising from transverse relaxation are not a major concern, the methods presented here may be useful alternatives to other triple-resonance E.COSY experiments in which the determination of ^3J couplings involving the $^{13}C^{\beta}$ nucleus is a priori excluded for serine and threonine residues.

Acknowledgements

We thank Dr. J.M. Schmidt for providing the software for the trace alignment procedure. The support from Prof. S.G. Mayhew (Department of Biochemistry, University College Dublin) with the expression and labelling of the *D. vulgaris* flavodoxin is gratefully acknowledged. We are indebted to Dr. Martin Walsh (EMBL, Hamburg) for making available the 1.7 Å X-ray structure of oxidized flavodoxin prior to

publication. This work was supported by a grant from the Deutsche Forschungsgemeinschaft (Ru 145/11-2).

References

Andersson, P., Gsell, B., Wipf, B., Senn, H. and Otting, G. (1998) *J. Biomol. NMR*, **11**, 279–288.

Archer, S.J., Ikura, M., Torchia, D.A. and Bax, A. (1991) *J. Magn. Reson.*, **95**, 636–641.

Blümel, M., Schmidt, J.M., Löhr, F. and Rüterjans, H. (1998) *Eur. Biophys. J.*, **27**, 321–334.

Brüschweiler, R. and Case, D.A. (1994) *J. Am. Chem. Soc.*, **116**, 11199–11200.

Bystrov, V.F. (1976) *Prog. NMR Spectrosc.*, **10**, 41–81.

Cowburn, D., Live, D.H., Fischman, A.J. and Agosta, W.C. (1983) *J. Am. Chem. Soc.*, **105**, 7435–7442.

Delaglio, F., Torchia, D.A. and Bax, A. (1991) *J. Biomol. NMR*, **1**, 439–446.

Emsley, L. and Bodenhausen, G. (1990) *Chem. Phys. Lett.*, **165**, 469–476.

Geen, H. and Freeman, R. (1991) *J. Magn. Reson.*, **93**, 93–141.

Goldman, M. (1984) *J. Magn. Reson.*, **60**, 437–452.

Griesinger, C., Sørensen, O.W. and Ernst, R.R. (1985) *J. Am. Chem. Soc.*, **107**, 6394–6396.

Griesinger, C., Sørensen, O.W. and Ernst, R.R. (1986) *J. Chem. Phys.*, **85**, 6837–6852.

Griesinger, C., Sørensen, O.W. and Ernst, R.R. (1987) *J. Magn. Reson.*, **75**, 474–492.

Grzesiek, S. and Bax, A. (1993) *J. Am. Chem. Soc.*, **115**, 12593–12594.

Hoch, J.C., Dobson, C.M. and Karplus, M. (1985) *Biochemistry*, **24**, 3831–3841.

Hu, S.-J. and Bax, A. (1997) *J. Am. Chem. Soc.*, **119**, 6360–6368.

Hu, S.-J. and Bax, A. (1998) *J. Biomol. NMR*, **11**, 199–203.

Jahnke, W., Baur, M., Gemmecker, G. and Kessler, H. (1995) *J. Magn. Reson.*, **B106**, 86–88.

Karplus, M. (1959) *J. Chem. Phys.*, **30**, 11–15.

Karplus, M. (1963) *J. Am. Chem. Soc.*, **85**, 2870–2871.

Kay, L.E., Keifer, P. and Saarinen, T. (1992) *J. Am. Chem. Soc.*, **114**, 10663–10665.

Kay, L.E., Xu, G.Y. and Yamazaki, T. (1994) *J. Magn. Reson.*, **A109**, 129–133.

Knauf, M., Löhr, F., Blümel, M., Mayhew, S.G. and Rüterjans, H. (1996) *Eur. J. Biochem.*, **238**, 423–434.

Löhr, F. and Rüterjans, H. (1995) *J. Biomol. NMR*, **5**, 25–36.

Löhr, F., Blümel, M., Schmidt, J.M. and Rüterjans, H. (1997) *J. Biomol. NMR*, **10**, 107–118.

Madsen, J.C. and Sørensen, O.W. (1992) *J. Magn. Reson.*, **100**, 431–436.

Madsen, J.C., Sørensen, O.W., Sørensen, P. and Poulsen, F.M. (1993) *J. Biomol. NMR*, **3**, 239–244.

Marion, D. and Wüthrich, K. (1983) *Biochem. Biophys. Res. Commun.*, **113**, 967–974.

Marion, D., Ikura, M., Tschudin, R. and Bax, A. (1989a) *J. Magn. Reson.*, **85**, 393–399.

Marion, D., Ikura, M. and Bax, A. (1989b) *J. Magn. Reson.*, **84**, 425–430.

Matsuo, H., Kupče, Ē., Li, H. and Wagner, G. (1996) *J. Magn. Reson.*, **B111**, 194–198.

Meissner, A., Duus, J.Ø. and Sørensen, O.W. (1997a) *J. Biomol. NMR*, **10**, 89–94.

Meissner, A., Duus, J.Ø. and Sørensen, O.W. (1997b) *J. Magn. Reson.*, **128**, 92–97.

Meissner, A., Schulte-Herbrüggen, T. and Sørensen, O.W. (1998a) *J. Am. Chem. Soc.*, **120**, 3803–3804.

Meissner, A., Schulte-Herbrüggen, T. and Sørensen, O.W. (1998b) *J. Am. Chem. Soc.*, **120**, 7989–7990.

Palmer III, A.G., Cavanagh, J., Wright, P.E. and Rance, M. (1991) *J. Magn. Reson.*, **93**, 151–170.

Schmidt, J.M., Ernst, R.R., Aimoto, S. and Kainosho, M. (1995) *J. Biomol. NMR*, **6**, 95–105.

Schmidt, J.M., Blümel, M., Löhr, F. and Rüterjans, H. (1999) *J. Biomol. NMR*, in press.

Schmieder, P. and Kessler, H. (1992) *Biopolymers*, **32**, 435–440.

Seip, S., Balbach, J. and Kessler, H. (1994) *J. Magn. Reson.*, **B104**, 172–179.

Shaka, A.J., Barker, P.B. and Freeman, R. (1985) *J. Magn. Reson.*, **64**, 547–552.

Shaka, A.J., Lee, C.J. and Pines, A. (1988) *J. Magn. Reson.*, **77**, 274–293.

Stockman, B.J., Richardson, T.E. and Swenson, R.P. (1994) *Biochemistry*, **33**, 15298–15308.

Stonehouse, J., Shaw, G.L., Keeler, J. and Laue, E.D. (1994) *J. Magn. Reson.*, **A107**, 178–184.

Tjandra, N., Szabo, A. and Bax, A. (1996) *J. Am. Chem. Soc.*, **118**, 6986–6991.

Wagner, G. (1990) *Prog. NMR Spectrosc.*, **22**, 101–139.

Wang, A.C. and Bax, A. (1995) *J. Am. Chem. Soc.*, **117**, 1810–1813.

Wang, A.C. and Bax, A. (1996) *J. Am. Chem. Soc.*, **118**, 2483–2494.

Watt, W., Tulinsky, A., Swenson, R.P. and Watenpaugh, K.D. (1991) *J. Mol. Biol.*, **218**, 195–208.

Wittekind, M. and Mueller, L. (1993) *J. Magn. Reson.*, **B101**, 201–205.

Zhu, G. and Bax, A. (1990) *J. Magn. Reson.*, **90**, 405–410.